Producing droplets in parallel microfluidic systems

V. Barbier, H. Willaime, and P. Tabeling
Theorie et microfluidique, ESPCI 10, rue Vauquelin, 75231 Paris, France

F. Jousse
Unilever Corporate Research, Colworth House, Sharnbrook, Bedfordshire MK44 ILQ, United Kingdom

(Received 30 December 2005; published 23 October 2006)

We study the dynamics of two microfluidic droplets emitters placed in parallel. We observe complex dynamical behavior, including synchronization, quasiperiodicity, and chaos. This dynamics has a considerable impact on the properties of the resulting emulsions: chaotic and quasi-periodic regimes give rise to polydispersed emulsions with poorly controllable characteristics, whereas synchronized regimes generate well-controlled monodispersed emulsions. We derive a dynamical model that reproduces the trends observed in the experiment.

DOI: 10.1103/PhysRevE.74.046306 PACS number(s): 47.61.−k, 05.45.Xt, 47.55.dd

Research efforts developed over the last few years have shown that microfluidic technology is remarkably well adapted for the handling, transport, and transformations of individual micrometric-sized droplets [1–5]. These capabilities allow new perspectives in the domain of emulsions. Today, one may envision new devices that exploit this technology, dedicated to elaborate emulsions with novel characteristics and properties. Microfluidic technology lays the foundations of a bottom-up approach to emulsion science that challenges the "top-down" techniques that typically handle large populations of droplets at each step of the industrial process. Nonetheless, the impact of the "new" technology will depend on its ability to deliver emulsions in quantities of practical significance. A single emitter built on a microfluidic chip typically conveys flow rates on the order of tens of microliters per minute, which is far too small to envisage industrial applications. Thus, it is necessary to parallelize droplet emitters to reach levels of practical interest. Nonetheless, by parallelizing droplet emitters, one couples fluidic oscillators. One issue is to know what dynamics the system will generate along with the characteristics of the emulsions that will be obtained. Previous theoretical studies on parallel microfluidic drop emitters have assumed stationarity [6] and therefore could not address this issue. Here, we study the most elementary parallelized system (two droplets emitters placed in parallel) and observe, at this stage, complex dynamical behavior involving synchronization, quasiperiodicity, and chaos. For some geometries, chaotic regimes occupy the entire phase space accessible to the experiment. The objective of the article is to report these findings and present a theoretical framework providing an interpretion of these observations. From a practical viewpoint, the phenomena we observed are important to consider for conceiving operational emulsion production units bearing on microfluidic technology.

The experimental system we are considering here is shown in Fig. 1. Water and oil feed two T junctions placed in parallel on the same chip. The droplets are produced at the two junctions, move downstream, and are eventually collected in a single microcanal. Flows are driven by syringe pumps (KDS Scientific) (we checked that imposing pressures instead of flow rates lead to similar results). There is one single entry for oil and two separate entries for water, which are each connected to an independent syringe pump. The channels are molded in PDMS (PolyDimethylSiloxane) using soft lithography technology. They are covered by a glass plate coated with a PDMS film so as to expose the fluids to surfaces with homogeneous hydrophobicity.

The microchannels have rectangular cross sections, 30 μm high and 100 μm wide; their lengths lie in the centimeter range. The fluids in use are tetradecane and a dilute fluorescein-water solution; flow rates range between 0 and 20 μl/min for oil and 0 and 10 μl/min for water. The system is observed by using epifluorescence videomicroscopy. The emission frequency, drop sizes, and water and oil flow rates in each branch are inferred from instantaneous measurements of the local light intensity, taken a few hundred micrometers downstream the T junctions. These local measurements were made by using a CCD camera. Acquisition times lie between hundreds of seconds (representing more than 300 drops) up to several hours. Various treatments of the time series are performed (Fourier transform, distribution of the drop sizes…). The electrical representation of our parallel system is shown in Fig. 1(b). The branches of the circuit are represented by electrical resistances. Here, the resistance R_o is constant, while R_s and R'_s are time-dependent quantities

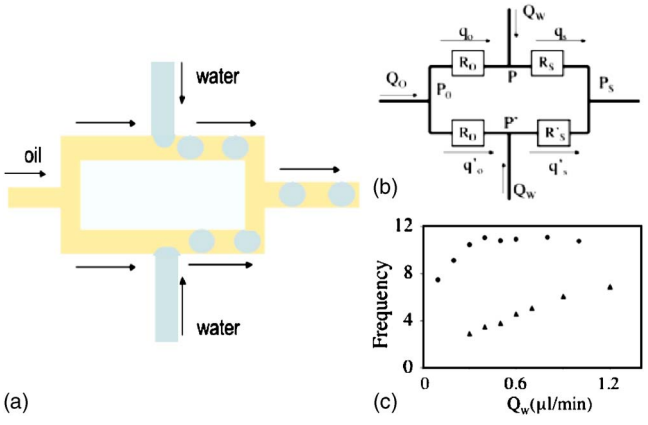

FIG. 1. (Color online) (a) Sketch of the parallelized system studied in the paper. (b) Equivalent electrical circuit of the microfluidic system. (c) Typical dispersion curves for isolated emitters with Q_0=1 (triangles) and 2 (circles) μl/mn.

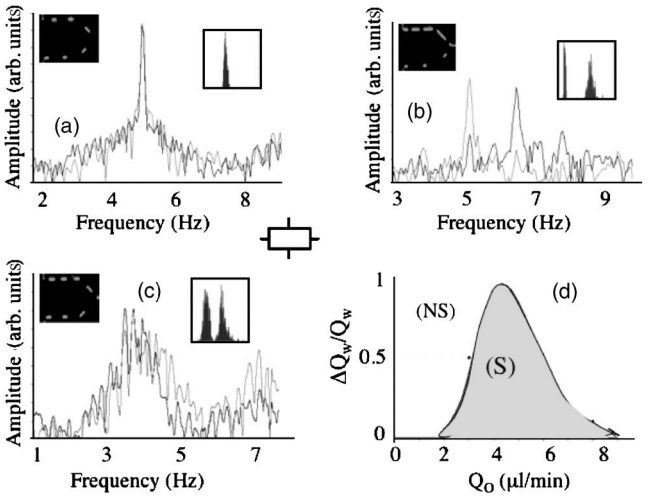

FIG. 2. (a)–(c) Local light intensity Fourier spectra, measured, respectively, in the upper (—) and lower branches (—) of the network, at 200 μm downstream the T junctions; inserts: corresponding sketches of the droplet sizes distributions: (a) Q_o=4 μL/min, Q_w=0.6 μL/min, Q'_w=0.5 μL/min; (b) Q_o=4 μL/min, Q_w =1.2 μL/min, Q'_w=0.5 μL/min; (c) Q_o=2.5 μL/min, Q_w =1.1 μL/min, Q'_w0.5 μL/min. (d) Ranges of existence of synchronized (S) and nonsynchronized (NS) regimes in a diagram $\delta Q_w/Q_w - Q_O$ for $Q_W+Q'_W$=1 μL/min (with $\delta Q_w = Q'_W - Q_W$).

since in each branch, water, and oil fractions change each time a droplet enters or leaves the branch.

We characterized each T junction separately. Typically, we found that the emission frequencies increase with the water and oil flow rates, forming a set of curves we call "dispersion curves." Examples of such curves are displayed in Fig. 1(c).

We now consider the system shown in Fig. 1(a) and concentrate on the case when the branches of the bridge have the same length. In this case, depending on the difference $\delta Q_w = Q_w - Q'_w$ and the oil flow rate Q_o, two different dynamical regimes are observed. The first one is synchronized (S): in this regime, the two emitters operate at the same frequency. The other regimes—non-synchronized (NS) regimes—includes two cases: quasi-periodic states in which the branches operate at several frequencies and chaotic regimes for which the light intensity spectra are composed of broadbands. An example of a synchronized regime is shown on Fig. 2(a) for δQ_w=0.1 μl/mn: on the Fourier spectra of the light intensity time series, one obtains sharp peaks located at the same frequency for each branch.

In the synchronized regimes, the emulsions are monodispersed and the corresponding mean standard deviations of the size distributions are on the order of 3% [see the insert of Fig. 2(a)]. An example of a quasi-periodic regime is shown in Fig. 2(b): here δQ_w is equal to 0.7 μl/min and the spectrum includes a sequence of discrete peaks. In such regimes, the dispersion of the droplet sizes typically reaches 8% on each branch. Nonetheless, the average sizes of the droplets substantially differ between the two branches, so that, as a whole, the dispersivity of the emulsion reaches levels on the order of 40%; this level is extremely sensitive to the flow conditions: it typically varies by 50% or so under the effect

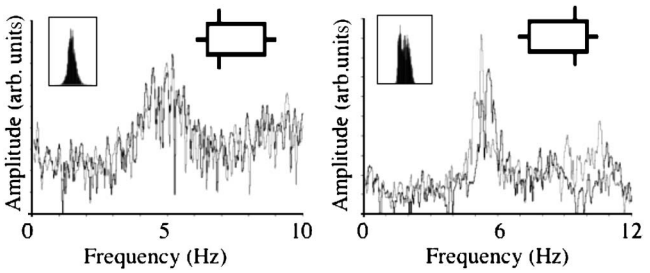

FIG. 3. Frequency spectra of the light intensity signal measured in each branch (— upper branch, — lower branch) and overall droplet size distributions in various conditions, for bridges with unequal branch lengths; (a) L_w/L_o=5; Q_o=4 μL/min; $Q_w = Q'_w$ =0.5 μL/min; (b) L_w/L_o=1/5; Q_o=4 μL/min; Q_w=0.5 μL/min, Q'_w=0.55 μL/min.

of a slight change of the flow rates. Finally, an example of a chaotic regime is shown in Fig. 2(c). In this case, the spectra are composed of broadbands that are typical of chaotic regimes. Here again, the size dispersions of the droplet sizes are large—they reach levels on the order of 30–60 %. The diagram showing the flow conditions under which these regimes are observed is shown in Fig. 2(d). Frequency locking states (S) occupy triangular regions. Outside the triangle, the regimes are nonperiodic (i.e., either quasi-periodic or chaotic).

Experiments performed for different bridge lengths revealed a spectacular dependence on the geometry. This is shown in Figs. 3(a) and 3(b). In a first case (L_s/L_o=5), synchronized regimes do not exist *even when* Q_w and Q'_w *are equal*. Instead, chaotic regimes take place in all conditions, giving rise to polydispersed emulsions with broad size distributions. Here also, the characteristics of these distributions evolve erratically with the flow conditions. This geometry thus essentially produces polydisperse emulsions with unpredictable properties.

In a second case where L_s/L_o=1/5 [Fig. 3(b)], quasi-periodic regimes are observed throughout the entire range of parameters investigated. Here again, the emulsion is polydispersed and the size dispersion is on the order of 40%.

We found the physical origin of the coupling by visualizing oil flow streamlines and tracking trajectories of individual droplets. We observed that in each branch, the oil flow streamlines substantially oscillated in time at frequencies close to droplet emission frequencies. This indicated that the oil flow rates vary in time in each branch. Because of the dispersion relation mentioned above, it follows that the droplet emission frequencies vary in time as well. Through this mechanism, each emitter parametrically forces the other. One may thus qualitatively understand that complex behavior takes place in our system [7,8].

We now model the dynamic behavior of the bridge. The goal here is not to provide a detailed account of the hydrodynamics of the system, but to capture its dynamics by building a model of minimal complexity. In this approach, we represent the fluidic emitters by Van der Pol oscillators: similarly as the fluidic emitters, Van der Pol oscillators are nonlinear, dissipative systems developing single frequency regimes [7]. In this analogy, it is natural to take the water

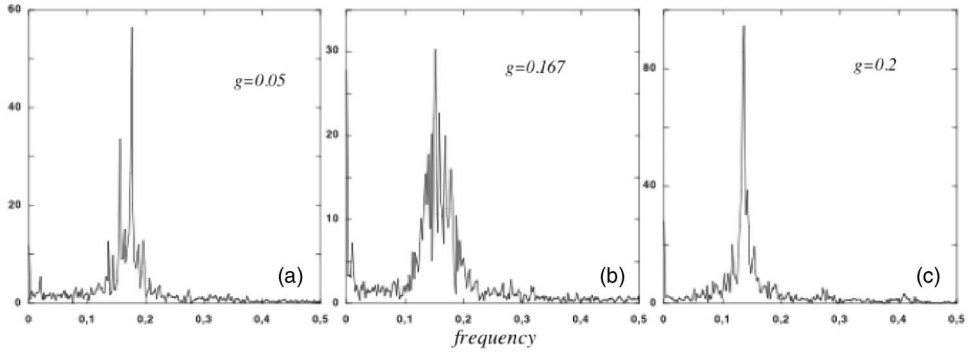

FIG. 4. Spectral amplitudes (i.e., square root of the density power spectra) of $\varphi+\varphi'$ obtained by resolving Eqs. (5) for $\omega_0=1$, $\omega_0'=1.123$ and different values of g. (a) $g=0.05$ (quasi-periodic regime); (b) $g=0.167$ (chaotic regime); (c) $g=0.2$ (synchronized regime).

fraction as the time-dependent variable in the Van der Pol system. The dynamical model we consider for our pair of emitters thus reads

$$\frac{d^2\varphi}{dt^2} - \lambda(1-\varphi^2)\frac{d\varphi}{dt} + \omega^2\varphi = 0,$$

$$\frac{d^2\varphi'}{dt^2} - \lambda(1-\varphi'^2)\frac{d\varphi'}{dt} + \omega'^2\varphi' = 0, \quad (1)$$

where φ and φ' are the temporal fluctuations of the water concentrations in the upper and lower branches, respectively, $\omega=2\pi f$ and $\omega'=2\pi f'$ are the angular frequencies at which the emitters operate and λ is a parameter. In our system, the emitter frequencies f and f' depend on the branch oil flow rates q_o and q_o'. By using the electrical representation shown in Fig. 1(b), one obtains the following expressions for q_o and q_o':

$$q_O = \frac{(R_S'+R_O)Q_O + R_S'Q_W' - R_SQ_W}{R_S+R_S'+2R_O}; \quad q_O' = Q_O - q_O. \quad (2)$$

As previously mentioned, R_s and R_s' depend on the water fractions held in the branches. Since water fractions change each time a droplet enters or leaves a branch, the two resistances fluctuate in time, and so do q_o, q_o' [see (2)]. This, in turn, forces the angular frequencies ω and ω' to vary in time. This is the parametric forcing mechanism we mentioned above. Following the work of Ref. [5], we postulate a linear relation between R_s and φ in the form $R_s=R_{s0}+a\delta R\,\varphi$, where a is a coefficient depending on the viscosity ratio between the continuous and dispersed phases and δR is a quantity characterizing the resistance variation produced by the gain or the loss of an isolated droplet in the upper branch. A similar relation holds for R_s' with the same factors a and δR but withφ' instead of φ. In the limit of small $\delta Q_w=Q_w'-Q_w$, and small a, the relations (2) can be rewritten as

$$q_o \approx \frac{Q_o}{2} + b(\varphi'-\varphi) + c\,\delta Q_W;$$

$$q_o \approx \frac{Q_o}{2} - b(\varphi'-\varphi) - c\,\delta Q_W, \quad (3)$$

where $b=\frac{a\delta R(Q_O+2Q_W)}{4(R_{S0}+R_O)}$ and $c=\frac{R_{S0}}{2(R_{S0}+R_O)}$ are dimensionless factors determined by expanding relations (2). One may proceed further by linearizing the dispersion relation $\omega(Q_0)$ around a reference solution ω_{00} obtained for φ, φ' $\delta Q_w=0$, implying $q_o=q_o'=Q_o/2$. We obtain

$$\omega \approx \omega_{00} + b\frac{\partial\omega}{\partial Q_o}(\varphi'-\varphi) + h\,\delta Q_W \approx \omega_0 + b\frac{\partial\omega}{\partial Q_o}(\varphi'-\varphi),$$

$$\omega' \approx \omega_{00} - b\frac{\partial\omega}{\partial Q_o}(\varphi'-\varphi) - h\,\delta Q_W \approx \omega_0' - b\frac{\partial\omega}{\partial Q_o}(\varphi'-\varphi), \quad (4)$$

with $h=c\,\partial\omega/\partial Q_O-\partial\omega/\partial Q_w$ and in which ω_0 and ω_0' are the two natural frequencies of the droplet emitters determined for $q_o=q_o'=Q_o/2$, $q_w=Q_w$ and $q_w'=Q_w'$, Finally, one obtains the following set of equations that defines our model:

$$\frac{d^2\varphi}{dt^2} - \lambda(1-\varphi^2)\frac{d\varphi}{dt} + \omega_0^2[1+r(\varphi'-\varphi)]\varphi = 0,$$

$$\frac{d^2\varphi'}{dt^2} - \lambda(1-\varphi'^2)\frac{d\varphi'}{dt} + \omega_0'^2[1-r'(\varphi'-\varphi)]\varphi' = 0 \quad (5)$$

in which r,r' are two coefficients defined by the following expressions:

$$r=\frac{g}{\omega_0}; \quad r'=\frac{g}{\omega_0'}; \quad g=\frac{a\delta R(2Q_W+Q_O)}{2\omega_{00}(R_{S0}+R_O)}\frac{\partial\omega}{\partial Q_O}, \quad (6)$$

g is a parameter that characterizes the coupling between the two emitters. Small g corresponds to weakly coupled emitters. According to (6), this can be achieved by increasing the resistances of the branches or designing the emitters so as their natural frequencies become independent of the oil flow rate. Upon increasing g, the coupling between the emitters is increased and synchronization between the emitters is favored. We computed Eqs. (5) for $\lambda=0.03$ (but other λ give similar behaviors), different values of g comprised between 0 and 0.25—this range is consistent with experimental estimates—and different ω_0' (fixing $\omega_0=1$). As a whole, we recover the behavior found for parametrically forced oscillators, i.e., resonance tongues separated by quasi-periodic regions and chaotic dynamics within regions, where the tongues tend to overlap [9]. Figure 4(a) shows a case where the coupling factor g is small and quasi-periodic regimes are obtained. As g is raised up synchronization takes place [an example is shown for $g=0.2$ in Fig. 4(c)]. For intermediate g, broadband spectra develop, indicating the presence of chaotic regimes [Fig. 4(b)].

These numerical findings are consistent with the experimental trends: in the experiment, raising up the branch resistances (either R_o or R_s) amounts to decrease g [see relation (6)]. The sequence of synchronized, broadband spectra, and quasi-periodic regimes we obtained by increasing the resistances of the branches is thus consistent with the sequence of regimes we found in the model. The diagram of Fig. 2(d) also receives a theoretical explanation: according to formula (6), and from the empirical knowledge of the dispersion curves, g reaches a maximum around $Q_o=0.5$ μl/min as the oil flow rate is varied. The triangular shape of Fig. 2(d) may thus be related to the fact that as we move around the apex, g becomes smaller and, consequently, the emitters tend to desynchronize.

To conclude, we observed complex dynamical behavior, including synchronization, quasiperiodicity, and chaos in an elementary parallel system dedicated to produce emulsions with improved throughput. We found that chaotic and quasi-periodic behavior enhance polydispersivity and jeopardize control while synchronization gives rise to well-defined monodispersed emulsions. We derived a model consistent with the experiment. This article provides guidance for the conception of devices using microfluidic technology to produce emulsions. The complexity of the dynamics shown in the present article may raise difficulties for the production of microfluidic-based emulsions. On the other hand, one may suggest that by using appropriate geometries, the production of monodispersed emulsions in quantities of practical interest is feasible.

We acknowledge CNRS and ESPCI for their financial support to this work. The work was done with the support of Unilever Grant No. CH1004-0436.

[1] T. Kawakatsu, Y. Kikuchi, and M. Nakajima, J. Am. Oil Chem. Soc. **74**, 317 (1997).
[2] T. Thorsen, R. W. Roberts, F. H. Arnold, and S. R. Quake, Phys. Rev. Lett. **86**, 4163 (2001).
[3] D. Link, S. Anna, D. Weitz, and H. Stone, Phys. Rev. Lett. **92**, 054503 (2004).
[4] R. Dreyfus, P. Tabeling, and H. Willaime, Phys. Rev. Lett. **90**, 144505 (2003).
[5] H. Song, J. Tice, and R. Ismagilov, Angew. Chem., Int. Ed. **42**, 767 (2003).
[6] Fabien Jousse, Guoping Lian, Ruth Janes, and John Melrose, Lab Chip **6**, 646 (2005).
[7] A. J. Lichtenberg and M. A. Lieberman, *Regular and Stochastic Motion*, Applied Math. Science 38 (Springer-Verlag, Berlin, 1983).
[8] J. Guckenheimer and P. Holmes, *Nonlinear Oscillations, Dynamical Systems and Bifurcations of Vector Fields*, Applied Mathematical Science 42 (Springer-Verlag, Berlin, 1990).
[9] H. Willaime, V. Barbier, L. Kloul, S. Maine, and P. Tabeling, Phys. Rev. Lett. **96**, 054501 (2006).